Collectivity against nucleon transfer in sub-barrier fusion of $^{12}C+^{194,198}Pt$

A. Shrivastava,[1,2] S. Kailas,[1] A. Chatterjee,[1] A. Navin,[1] A. M. Samant,[3] P. Singh,[1] S. Santra,[1] K. Mahata,[1] B. S. Tomar,[4] and G. Pollarolo[5]

[1]*Nuclear Physics Division, Bhabha Atomic Research Centre, Mumbai 400 085, India*

[2]*Gesellschaft für Schwerionenforschung (GSI), D-64291 Darmstadt, Germany*

[3]*Instituto Nazionale di Fisica Nucleare, Laboratory Nazionali di Legnaro, I-35020 Legnaro, Italy*

[4]*Radiochemistry Division, Bhabha Atomic Research Centre, Mumbai 400 085, India*

[5]*Dipartimento di Fisica Teorica, Università di Torino, Via Pietro Giuria I, I-10125 Torino, Italy*

(Received 27 November 2000; published 2 April 2001)

In order to determine the relative importance of the role played by inelastic excitations and transfer channels of the colliding nuclei, in near-barrier fusion enhancement, the fusion cross sections have been measured for $^{12}C+^{194,198}Pt$ in the energy range of $0.9 \leqslant E/V_B \leqslant 1.2$. Additional data of quasielastic and nucleon(s)-exchange cross sections have also been measured at an energy of $1.2V_B$. The strength of transfer form factors required for the simplified coupled-channels calculations has been obtained from the transfer reaction measurements using a semiclassical approach and calculations based on complex WKB approximations. Coupled-reaction-channels calculations have been performed to explain the complete data set that included fusion, quasielastic, and transfer cross sections. The dominant contributions to the enhancement of fusion cross section compared to a one-dimensional barrier-penetration model arise from coupling to inelastic channels. It has been shown for the first time that the lighter isotope (^{194}Pt) of a given nuclide that has a relatively larger collectivity (β_λ) and a larger neutron separation energy compared to the heavier isotope (^{198}Pt), exhibits larger enhancement of fusion cross section. The experimental fusion-barrier distributions were obtained from fusion and quasielastic scattering data.

DOI: 10.1103/PhysRevC.63.054602 PACS number(s): 25.70.Jj, 25.70.Hi

I. INTRODUCTION

Enhancement of fusion cross sections (σ_{fus}), broadening of compound nuclear l distributions, and the threshold anomaly in elastic scattering at energies around the barrier are all related phenomena and arise due to the coupling of the relative motion with various degrees of freedom of the colliding nuclei [1]. The enhancement of fusion cross section in comparison to the prediction of a one-dimensional barrier-penetration model is known to increase with increasing deformation of the projectile/target and decrease of separation energy of the neutron (S_n) that is transferred between the colliding nuclei. Studies made with a fixed projectile on different isotopes have found a larger enhancement of fusion for the heaviest target isotope and correlation with positive Q-valued transfer reactions [1–6]. In the majority of cases studied across an isotopic series (except Ref. [5]), the target deformation increases while the neutron separation energy decreases with the increase of isotopic mass. Smaller values of neutron separation energy lead to relatively more positive Q-valued neutron-transfer reactions. Since the factors described above lead to larger enhancement in fusion cross section for the heaviest target isotope, it is difficult to isolate the role of transfer channels from inelastic excitations unambiguously in influencing the fusion process. Recent experiments selected nuclei with specific properties to study the relative importance of inelastic excitations against neutron transfer reactions in sub-barrier fusion enhancement [5–8]. In $^{40}Ca+^{90,96}Zr$ [6], both $^{90,96}Zr$ have similar nuclear structure but different neutron-transfer Q values. The neutron transfer channels in $^{40}Ca+^{90}Zr$ system have negative Q values. The very large enhancement observed in $^{40}Ca+^{96}Zr$ was attributed to strong coupling of sequential multinucleon (positive Q-valued) transfer channels. The lighter isotope of Ti in $^{40}Ca+^{46,48,50}Ti$ systems [5] is more deformed while transfer reactions with the heavier target have larger positive Q values. The heaviest isotope, though least deformed showed more enhancement in fusion cross section at energies near the barrier for this case as well. The larger fusion enhancement observed in $^{32}S+^{110}Pd$ [7] compared to $^{36}S+^{110}Pd$ was again shown to be related to larger neutron pickup transfer cross sections. However, the fusion data for $^{40}Ca+^{116,124}Sn$ [8] did not show any isotopic dependence. In a recent experiment with $^{36}S+^{90,96}Zr$ [9], larger sub-barrier fusion enhancement was observed for $^{36}S+^{96}Zr$. For the Pt isotopes with increasing neutron number the heavier isotope (^{198}Pt) approaches the neutron magic number and hence it is more spherical than the lighter isotope (^{194}Pt). Further S_n is smaller and the transfer Q values are more positive for the heavier target (Table I). This presents a situation similar to Ref. [5] where it was possible to isolate the role of transfer and inelastic couplings in the sub-barrier fusion enhancement within the framework of coupled channels formalism. If collectivity is important, $^{12}C+^{194}Pt$ should exhibit more en-

TABLE I. Deformation parameters (β_2, β_3), excitation energies (E_x), neutron separation energies (S_n), and neutron transfer Q values for $^{12}C+^{194,198}Pt$.

Nucleus	β_2	$E_x(2^+)$ (MeV)	β_3	$E_x(3^-)$ (MeV)	S_n (MeV)	$Q(+1n)$ (MeV)	$Q(+2n)$ (MeV)
^{194}Pt	0.15	0.328	0.13	1.43	8.4	-3.4	-1.48
^{198}Pt	0.11	0.407	0.10	1.5	7.6	-2.6	-0.28

hancement and if transfer couplings are dominant then $^{12}C + ^{198}Pt$ should show larger enhancement in fusion cross sections at near-barrier energies. However, as compared to Ref. [5] the systems under the current study are more asymmetric and have negative Q values for the nucleon transfer channels (except for the two-neutron pickup channel with a value close to zero for $^{12}C + ^{198}Pt$), the influence of the transfer channels on sub-barrier fusion may be less pronounced in the present case.

To understand the influence of nuclear structure in the fusion process at near-barrier energies it is important to make a complete study of various reaction channels. There are very few cases in the literature where a complete data set of the required type exists. For coupled channels (CC) calculations the inelastic form factors can be calculated using closed expressions [10,11] obtained from collective models. In the case of transfer reactions knowledge of the spectroscopic factors is required to obtain the strength of transfer form factors. The transfer strength is usually treated as a parameter in the absence of this information and is adjusted to reproduce the fusion data. The role of transfer couplings can be studied quantitatively by measuring the transfer data, which in turn require quasielastic (QE) angular distribution measurements to obtain the optical model parameters.

In this work we report the measurement of fusion cross sections, compound-nucleus average angular momenta derived from the measured evaporation residue (ER) ratios at near-barrier energies and associated measurements of few-nucleon transfer along with the quasielastic angular distributions at an energy of 73.5 MeV. The transfer angular distributions have been analyzed using an improved semiclassical approach [12] to extract the strength of the transfer form factor required for coupled channels calculations. A calculation based on the complex WKB (CWKB) approximation [13] has been performed to explain the transfer angular distribution and extract the strength of the transfer form factors. Results of the fusion measurements have been compared with simplified coupled-channels calculations [14] incorporating inelastic and transfer couplings. The fusion-barrier distributions have been deduced both from the fusion-excitation function [15,16] and the QE excitation function measured at backward angles [17,18] and have been compared with the coupled channels calculations incorporating higher-order coupling terms [19]. A complete coupled-reaction-channels calculation has been performed to explain simultaneously the elastic (includes target inelastic states), transfer, and fusion data.

This paper is organized as follows. In Sec. II the experimental setup together with the experimental data are presented. In Sec. III A, analysis of fusion data along with the transfer data is given. Semiclassical and complex WKB methods of treatment of transfer channels are discussed. The deduced fusion barriers are discussed in Sec. III B. The detailed coupled-reaction-channels analysis is presented in Sec. III C followed by conclusions in Sec. IV.

II. EXPERIMENTAL DETAILS AND RESULTS

Fusion-excitation functions for $^{12}C + ^{194,198}Pt$ systems have been determined by summing the measured evaporation residue and fission cross sections [20–22]. The measurements for the evaporation residues have been made by counting off-line gamma activity. ^{12}C beams were obtained from the 14UD BARC-TIFR Pelletron accelerator facility at Mumbai and the measurements were carried out in the energy range of 55–75 MeV. For the off-line measurements, self-supporting rolled foils of ^{194}Pt (97% enriched and 1 mg/cm^2 thick) and ^{198}Pt (97% enriched and 1.3 mg/cm^2 thick) were used as targets. The targets were backed by Al-catcher foils of thickness 2 mg/cm^2 to stop the residues. The typical beam currents were around 20 pnA. The mean charged-state of the beam after passing through the target was obtained from measured charge state distributions [23]. The small time variation of the beam current was taken into account for estimating evaporation-residue cross sections. The γ activity was measured using efficiency-calibrated HpGe detectors of active volumes 60, 80, and 125 cm^3. For improved accuracy and to remove any interference of γ rays arising from any other source, the ER cross sections were deduced after following the decay for several half-lives and using more than two gamma-ray transitions for identifying each ER. In some cases, the cross-section values were confirmed by following the decay of the daughter nucleus. The statistical error on ER cross sections is $\approx 1-3\,\%$ at higher energies and at the lowest energies it is 5–8 %. The errors arising from uncertainties in branching ratio of the γ decay and efficiency of the HPGe detector is 3–5 %. The evaporation-residue cross sections are shown in Fig. 1 [22].

Fission cross sections for $^{12}C + ^{194,198}Pt$ have been measured in the energy range from 55 to 85 MeV using three surface-barrier telescopes. The details of the experimental

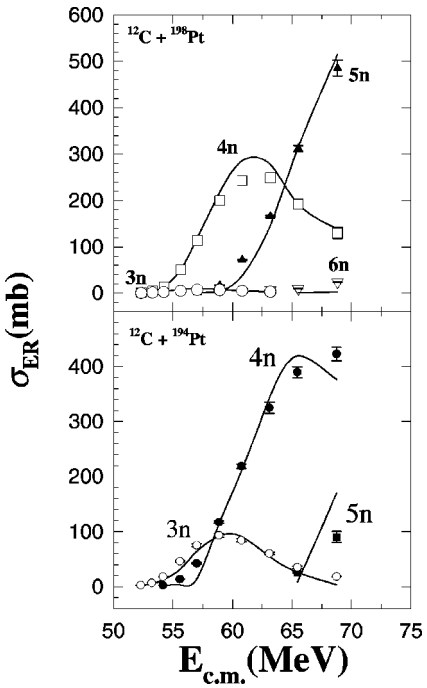

FIG. 1. The measured evaporation-residue excitation functions for systems $^{12}C + ^{194,198}Pt$. Different neutron-evaporation channels are indicated. Continuous curves are a result of statistical model calculations.

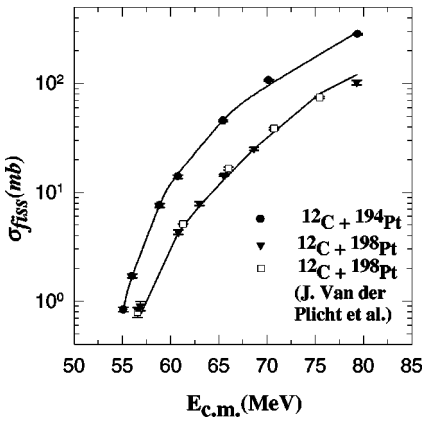

FIG. 2. The measured fission excitation function for systems $^{12}C+^{194,198}Pt$. Continuous curves are a result of the statistical model calculations. Along with the present data, the data from Ref. [24] are also shown for system $^{12}C+^{194}Pt$.

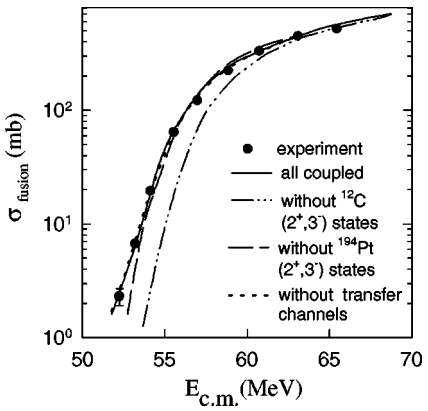

FIG. 3. Fusion excitation function for $^{12}C+^{194}Pt$. The experimental points are represented by filled circles. Solid curve is the result of coupled-reaction channels (CRC) calculation using the code FRESCO [36]. The dashed-dot curve and long-dashed curves are obtained when projectile and target inelastic states are not included in the calculation, respectively. The dotted curves result when transfer channels are not coupled.

setup for fission measurement are given in Ref. [22]. Angular distributions for fission fragments have been measured in the range of 80°–170° deriving the trigger signal for the data acquisition system from ΔE detectors. Relative solid angles between the detectors were obtained by measurements at overlapping angles. The data collected as two-dimensional spectra showed a clear separation of the fission events from the quasielastic events. Results of the fission measurement are displayed in Fig. 2 along with data from the literature [24].

At lower energies the fusion cross section is determined entirely by neutron evaporation channels. Contributions from charged-particle evaporation channels at near-barrier energies are estimated from statistical model (SM) calculations to be negligible ($<1\%$) [22]. At higher energies, contributions from the charged-particle evaporation channels to fusion are estimated to be less than 10% of the total fusion cross section. The measured fusion cross sections are tabulated in Table II and are shown in Figs. 3 and 4. The first moments of the compound nuclear angular momentum distributions for $^{12}C+^{194,198}Pt$ have been derived from the ratios of the measured ERs using the SM code PACE [25] (Fig. 5). The procedure followed [26] utilizes the fact that the relative fractionation of ERs resulting from the decay of a compound nucleus at a given excitation energy depends upon the initial angular momentum distribution (along with the density of final states and penetration factor).

The angular distributions for one- and two-neutron pickup and one- and two-proton stripping channels have been measured at 73.5 MeV for $^{12}C+^{194,198}Pt$. The measurements have been made using three surface-barrier telescopes with the E detectors of thickness 300 μm each and ΔE detectors of thicknesses 35, 40, and 46.8 μm. The angular range covered during the experiment was from 40° to 125° that corresponds to the distance of closest approach (D_0) for a Coulomb trajectory from 18.9 fm to 10.5 fm. The angular spread $\Delta\theta$ was kept small (0.6°). A 300-μm Si surface-barrier detector placed at 30° with respect to the beam direction was used for normalization. The total energy E was obtained by summing signals from the ΔE and E detectors after performing a proper gain matching of the detector signals. Particle identifier (PI) vs E spectra were generated using the algo-

TABLE II. Fusion cross sections (σ_{fus}) for $^{12}C+^{194,198}Pt$. The error due to the counting statistics alone is indicated.

	$^{12}C+^{194}Pt$	$^{12}C+^{198}Pt$
E_{lab} (MeV)	σ_{fus} (mb)	σ_{fus} (mb)
55.5	2.3±0.15	1.6±0.07
56.5	6.7±0.2	5.5±0.11
57.5	19.6±0.6	15.6±0.25
59.0	62.0±1.8	55.5±1.5
60.5	126.0±4.0	125.0±4.0
62.5	229.6±7.0	230.2±7.0
64.5	330.8±10.0	332.0±10.0
67.0	435.0±14.0	437.0±14.0
69.5	535.3±16.0	538.0±17.0
73.0	660.0±20.0	670.0±20.0

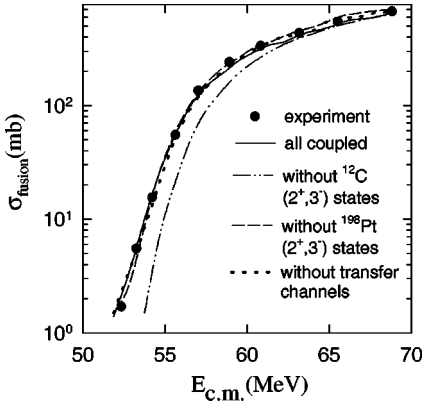

FIG. 4. Same as Fig. 1, for $^{12}C+^{198}Pt$.

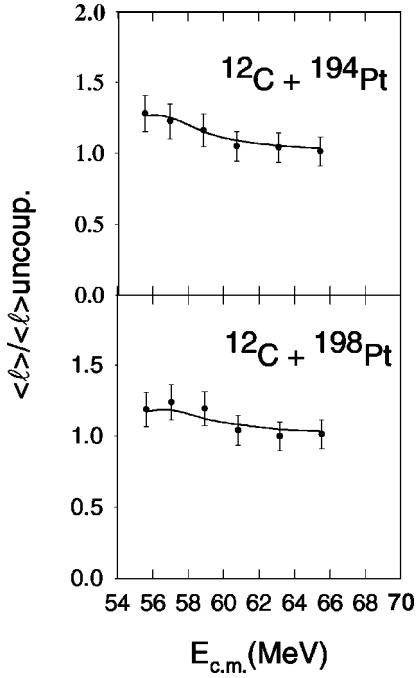

FIG. 5. Average of the CN spin distribution for $^{12}C+^{194,198}Pt$. Filled circles are the experimental points. Solid curves are obtained using the CC code CCDEF [14]. The experimental and calculated values are plotted after dividing by corresponding uncoupled values.

rithm $M^{a-1}z^2 \propto (\Delta E + E_{res})^b - E_{res}^b$, with $b=1.65$. In this expression ΔE and E_{res} are energies deposited by the particle in ΔE and E detectors, respectively. The numerical value of a was obtained using tables of Northcliff and Schilling [27]. The results of transfer measurements are shown in Figs. 6–9. Elastic scattering (including low-lying states of the target) angular distributions at energy 73.5 MeV are shown in Figs. 10 and 11 for the two systems.

The measurements for quasielastic excitation function at fixed angles for obtaining the barrier distribution have been

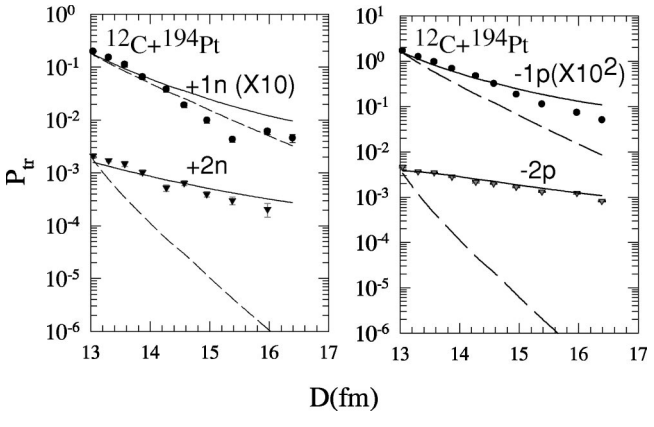

FIG. 6. Transfer probabilities (P_{tr}) plotted as a function of the distance of closest approach (D) for $^{12}C+^{194}Pt$ at $E_{lab}=73.5$ MeV. The continuous and the dashed curves are results of the calculations made including and not including the nuclear branch, respectively.

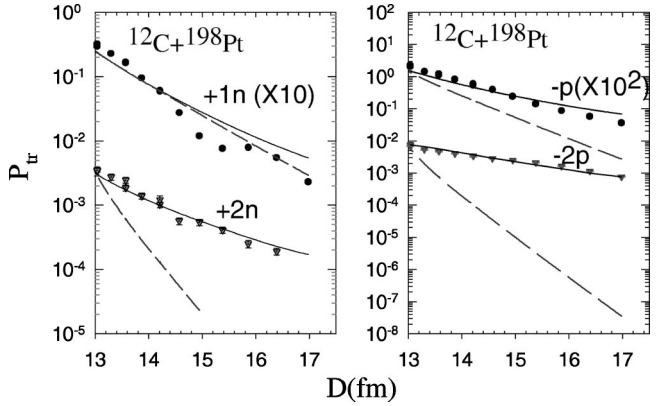

FIG. 7. Same as Fig. 6, for $^{12}C+^{198}Pt$.

made using three surface-barrier telescopes ($\sim\Delta E=12$ μm, $E=300$ μm) covering an energy range of 54–75 MeV, in steps of 1 MeV. A monitor detector was kept at 30° for normalization purposes. The measurements have been made with detector telescopes placed at fixed angles of 130°, 150°, and 170°.

III. ANALYSIS AND DISCUSSION

The fusion data have been analyzed within the framework of simplified coupled channels and exact coupled-reaction-channels models. For the simplified coupled-channels calculations the strength of transfer form factors (F_0) have been extracted from the measured transfer data [12,13]. In the case of exact coupled-channels calculations, the spectroscopic factors for specific states have been obtained from the literature [28]. The average angular momentum values extracted from the experiment have been compared with the calculations using simplified CC approach discussed below.

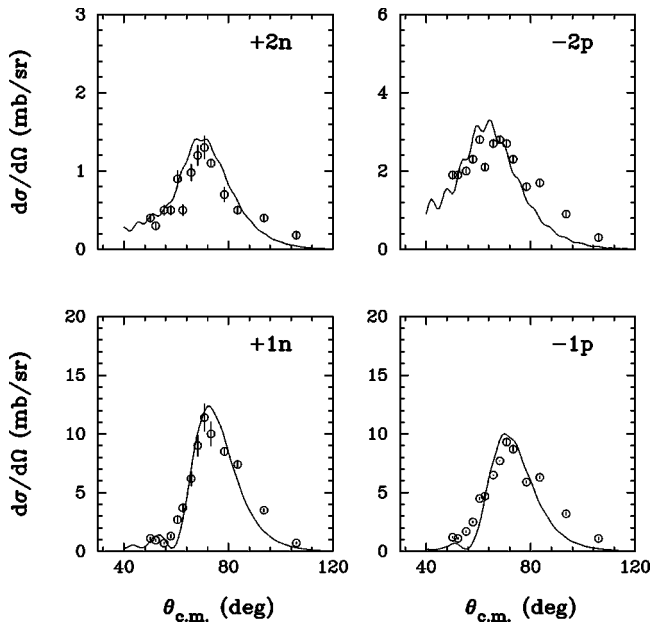

FIG. 8. Transfer angular distribution for $^{12}C+^{194}Pt$. The continuous curves are results of the CWKB calculations.

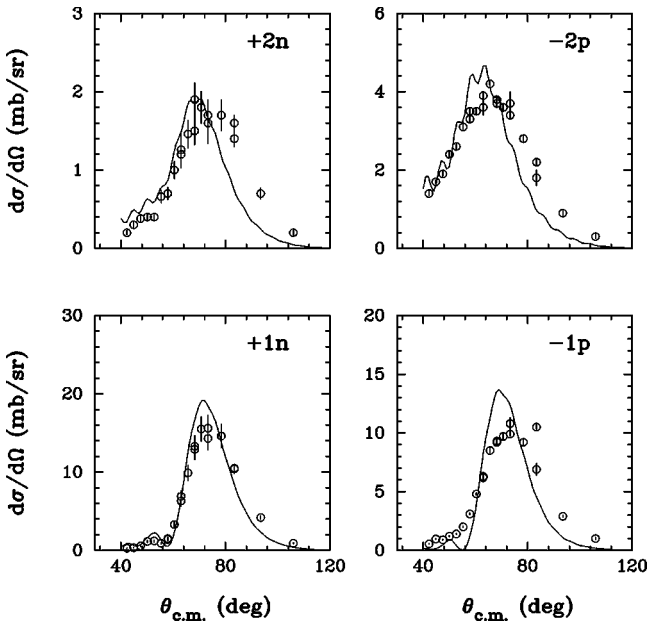

FIG. 9. Same as Fig. 8, for $^{12}C+^{198}Pt$.

A. Simplified coupled-channels calculations for fusion

In the simplified coupled-channels model proposed by Dasso *et al.* [29] fusion cross section is obtained by calculating transmission through the barriers that are modified by coupling of the incident channel to the other direct reaction channels. The calculations have been carried out using the code CCDEF [14], which is a modified version of the code CCFUS [30]. The geometry of the nuclear potential for the calculation has been obtained from the global Winther parametrization for Woods-Saxon potentials [31]. The depth of the nuclear potential was varied to reproduce the high-energy experimental fusion cross sections before including couplings to the nonelastic states.

(a) Coupling to inelastic channels. The inelastic states of targets and projectile have been coupled using the vibrational model, calculating the coupling strength from the collective model. The single-phonon 2^+ and 3^- states of the target and

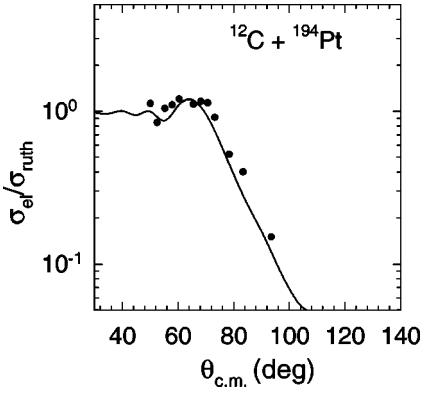

FIG. 10. Elastic scattering (includes low-lying states of the target) angular distribution measured at $E_{lab}=73.5$ MeV for $^{12}C+^{194}Pt$. Solid curve is the result of CRC calculation using the code FRESCO [36].

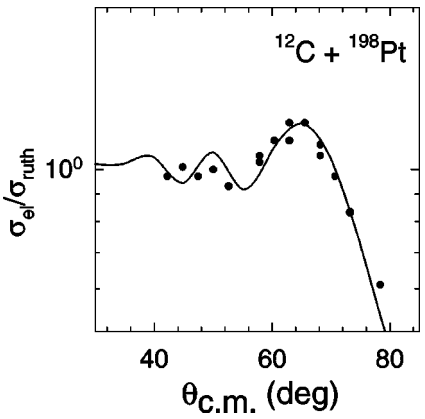

FIG. 11. Same as Fig. 10, for $^{12}C+^{198}Pt$.

2^+ state of the projectile ($\beta_2=0.59$ and $E_x=4.44$) have been included in the calculation. The deformation parameters and corresponding excitation energies [11] for $^{194,198}Pt$ are listed in Table I.

(b) Coupling to transfer channels. The strength of transfer form factor F_0 has been obtained using two different methods. In the first method the slope anomaly in transfer probability (P_{tr}) is explained by including both the nuclear and the Coulomb branches of the classical deflection function [12]. The nuclear potential required for this calculation has been obtained by fitting the QE scattering angular distribution using the optical model code SNOOPY [32]. The QE scattering events have been obtained by summing elastic, inelastic, and Q-integrated transfer channels ($+1n,+2n,-1p,-2p$). The semiclassical calculations for one- and two-neutron pickup channels and one- and two-proton strip-off channels for $^{12}C+^{194,198}Pt$ systems are shown in Figs. 6 and 7, respectively. Also shown in these figures are results using only the Coulomb branch of the deflection function. It can be seen clearly that with the Coulomb branch alone, the transfer probability cannot be explained for two-nucleon transfer reactions. The transfer strengths F_0 have been extracted from transfer probabilities using a semiclassical model [33–35] and are listed in Table III. The form factor is assumed to have the form $F(r)=F_0e^{\alpha(r-R_B)}$ for $r>R_B$, where F_0 is the value at the barrier radius. The slope parameter α is written as $\alpha=(1/\hbar)(2\mu B)^{1/2}$, where μ and B are the reduced mass and binding energy corrected for Coulomb effects (for charged particles) of the transferred particle(s) in the target and projectile. Since discrete states could not be resolved, Q-integrated probability for each of the transfer channels has been obtained. Further, it has been assumed that F_0 is constant over the range of states of interest.

In the second approach [13], the relative motion between the reactants has been treated in CWKB approximation for $^{12}C+^{194,198}Pt$. The strength of transfer form factor is obtained after explaining the transfer angular distribution. The transfer cross sections are obtained in the CWKB approximation starting from the conventional distorted-wave Born approximation and assuming that the transfer takes place between the entrance and exit channel. The geometry of nuclear potentials used for calculating the phase shifts have been obtained from Winther parametrization [31]. The depth

TABLE III. Ground-state Q value (Q_{gg}) and strength of the form factor (F_0) at the barrier radius, extracted using semiclassical method (SM) and calculations with CWKB approximation.

Channel	Q_{gg} (MeV)	F_0(SM) (MeV)	F_0(CWKB) (MeV)
$^{12}C+^{194}Pt$			
+1n	-3.425	0.61±0.07	0.66±0.08
+2n	-1.484	0.37±0.06	0.26±0.04
-1p	-10.9	0.45±0.05	0.41±0.05
-2p	-15.5	0.52±0.05	0.45±0.05
$^{12}C+^{198}Pt$			
+1n	-2.6	0.64±0.08	0.86±0.10
+2n	-0.28	0.33±0.04	0.34±0.04
-1p	-9.50	0.50±0.06	0.35±0.05
-2p	-15.5	0.60±0.07	0.59±0.06

of the potential was varied to reproduce the experimental angular distributions. The same potential was used to calculate the differential cross sections for neutron transfer $(+1n,+2n)$ and proton transfer $(-1p,-2p)$ reactions in $^{12}C+^{194,198}Pt$. Results of the calculation are shown in Figs. 8 and 9 for $^{12}C+^{194,198}Pt$. The F_0 values deduced from this analysis are listed in Table III. It can be noted from Figs. 6–9 and Table III that even though the transfer cross sections are significantly different for the two systems, the corresponding F_0 values are similar within the experimental errors for the respective transfer channels. The two sets of F_0 values from the two methods do not differ significantly from each other. This implies that absorption effects are not very important in the treatment of transfer channels.

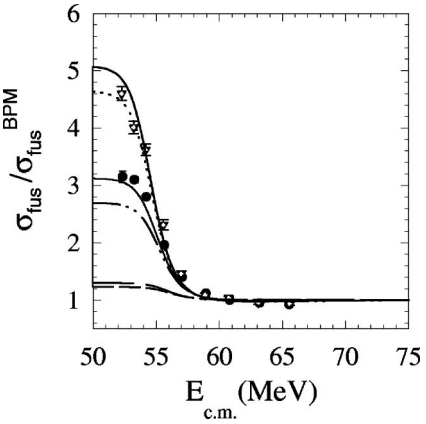

FIG. 12. The CC calculations obtained by coupling inelastic channels (dotted and dashed-dot curves for $^{12}C+^{194,198}Pt$, respectively) and transfer channels (dashed and long-dashed curves for $^{12}C+^{194,198}Pt$, respectively) separately are plotted as a function of center-of-mass energy. The cross sections are divided by the values obtained with one-dimensional barrier-penetration model prediction. Ratio of the experimental σ_{fus} (triangles and circles are, respectively, for $^{12}C+^{194,198}Pt$) and that from the coupled-channels calculation with all channels coupled (solid curve) to the σ_{fus} obtained from the one-dimensional barrier-penetration model is also shown.

TABLE IV. The fusion-barrier height, position, and curvature for $^{12}C+^{194,198}Pt$.

System	V_B (MeV)	R_B (fm)	$\hbar\omega$ (MeV)
$^{12}C+^{194}Pt$	55.90	11.31	4.84
$^{12}C+^{198}Pt$	55.90	11.31	4.79

The influence of inelastic and transfer channels in enhancing the fusion cross section has been studied by coupling inelastic and transfer channels separately in the CC calculations. Shown in Fig. 12 are the fusion cross sections resulting from these calculations plotted after dividing by the values obtained from one-dimensional barrier-penetration model at the corresponding energies. This figure shows that coupling to collective states is the dominant mechanism for fusion enhancement in the Pt isotopes with ^{12}C projectile. Proton transfer channels, due to their large negative Q values, were found to have a negligible effect on fusion enhancement. The height (V_B), position (R_B), and curvature ($\hbar\omega$) of the uncoupled barriers for the two systems are listed in Table IV. The results of CCDEF calculations for the mean value of the CN angular momentum distribution are displayed as solid curves in Fig. 5.

In Fig. 12, the ratio of experimental fusion cross section to the prediction of one-dimensional barrier-penetration model is plotted as a function of center-of-mass energy for $^{12}C+^{194,198}Pt$. From this figure it can be seen that the enhancement of fusion cross section is significantly higher for the more collective ^{194}Pt target as compared to that for ^{198}Pt. This in essence implies in a model-independent way that collective degrees of freedom are dominant in influencing near-barrier fusion in the present case.

B. Fusion barrier distribution

In the earlier section the enhancement in σ_{fus} and broadening of angular-momentum distribution at sub-barrier energies have been explained on the basis of coupled-channels calculations based on an eigenchannel approach. A more

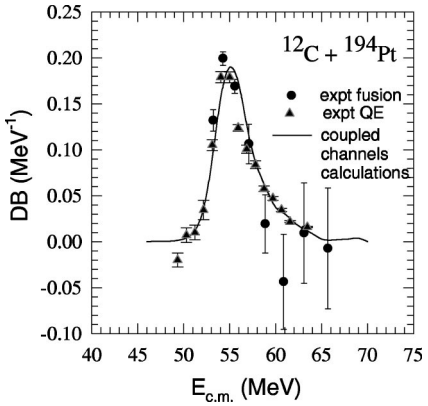

FIG. 13. Barrier distribution obtained from the QE data (filled triangles) and fusion data (filled circles) for $^{12}C+^{194}Pt$. The solid curve is result of CCDEF [14] calculations.

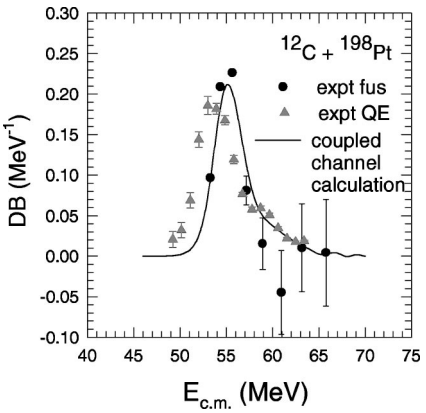

FIG. 14. Same as Fig. 13, for $^{12}C + ^{198}Pt$.

sensitive way for displaying the fusion data is the second derivative of the product $\sigma_{fus} \times E$, with respect to the energy, in general identified as the distribution of fusion barriers (DB) [15,16]. Following the method of Refs. [15,16], the barrier distribution has been extracted from the fusion-excitation functions measured for $^{12}C + ^{194,198}Pt$ in the energy range of $55 < E < 74$ MeV. From Figs. 13 and 14 it is seen that the DB for $^{12}C + ^{198}Pt$ is marginally compressed and the peak is slightly shifted toward higher energies as compared to $^{12}C + ^{194}Pt$. The solid curve is obtained from the simplified coupled-channels calculation described in Sec. III A with the energy step-size of 1 MeV. The transfer channels are found to have a negligible effect on the shape of the DB.

Using the approach suggested in Ref. [17], the DB was also obtained from the energy derivative of the quasielastic scattering cross sections. The results are displayed in Fig. 13 and Fig. 14 for the data taken at the scattering angle of 170°. The experimental DB from the fusion data and from the CC calculations are in good agreement with each other for both $^{12}C + ^{194,198}Pt$ (Figs. 13 and 14). The experimental DB obtained from the two different methods are in reasonable agreement for $^{12}C + ^{194}Pt$ while for $^{12}C + ^{198}Pt$ the DB from the QE data is broader in shape. A similar behavior was observed in Ref. [5].

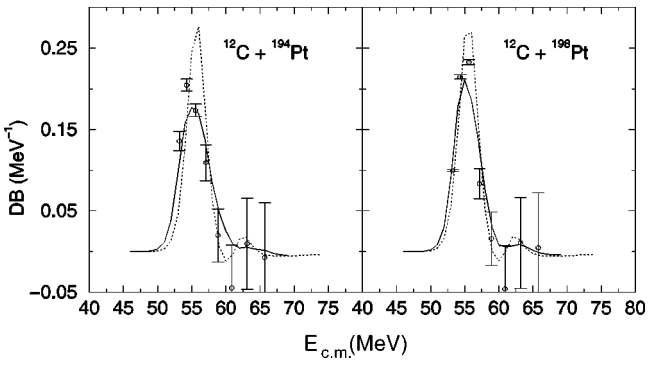

FIG. 15. Comparison of the barrier distribution obtained from all-order CC calculations with the experimental values for $^{12}C + ^{194,198}Pt$. The dotted curve is obtained when only projectile inelastic 2^+ state is coupled. The solid curve is obtained after coupling 2^+ state of projectile and 2^+ and 3^- states of the target.

TABLE V. Particle and hole states for proton stripping and neutron pickup considered in the calculations. C^2S is the spectroscopic factor.

Nucleus	J^π	E^*(MeV)	$\sqrt{C^2S}$
^{13}C	$1/2^-$	0.0	1.2
	$1/2^-$	3.09	0.9
^{11}B	$3/2^-$	0.0	1.9
^{193}Pt	$1/2^-$	0.0	1.2
	$3/2^-$	0.016	1.7
	$13/2^+$	0.15	2.2
^{197}Pt	$1/2^-$	0.0	0.7
	$3/2^-$	0.07	0.7
	$3/2^-$	0.09	0.8
	$5/2^-$	0.053	1.6
	$13/2^+$	0.39	2.4
^{195}Au	$3/2^+$	0.0	0.4
	$7/2^-$	1.59	1.7
^{199}Au	$3/2^+$	0.0	0.5
	$1/2^+$	0.08	0.5
	$1/2^+$	0.82	0.60

A coupled-channels calculation including higher-order coupling terms has been performed as proposed in Ref. [19]. Results of the calculation taking the energy step-size of 1 MeV are shown in Fig. 15. The dotted line is obtained by coupling only the 2^+ state of ^{12}C. For $^{40}Ca + ^{194}Pt$ system a higher energy peak was observed due to projectile excitation. In the present work with ^{12}C projectile the weight of the second peak is very small as compared to the $^{40}Ca + ^{194}Pt$ case. This weight gets redistributed when other states (2^+ and 3^- states of the target) are coupled (solid lines).

C. Coupled-reaction channels analysis

In the simplified CC calculations described above, only the fusion data are explained. In order to achieve a complete understanding of the fusion dynamics, it is necessary to explain other reaction processes like elastic scattering and direct reactions along with fusion. A complete coupled-reaction channels (CRC) calculation using the code FRESCO [36] has been performed to explain the fusion, elastic scattering (plus inelastic to low lying target states) and transfer reaction (one neutron pickup and one-proton stripping) data. The potential parameters that explain the elastic, transfer, and fusion data measured at a high energy (73.5 MeV) for $^{12}C + ^{194,198}Pt$ have been used to calculate fusion cross sections over the range of energies around the fusion barrier.

The four inelastic states coupled to the entrance channel are the 2^+, 3^- states of the projectile and target. The two transfer partitions included in the calculations correspond to one-neutron pickup and one-proton stripping channels. All the nonelastic channels are coupled to the entrance channel only. The inelastic states have been treated as collective (vibrational). The spectroscopic factors (C^2S) for transfer channels used in the calculations are listed in Table V [28]. Range and diffuseness of the real part of the optical-model potential have been calculated using the semiempirical parametrization of folding-model potentials given by Broglia

TABLE VI. Optical model parameters for $^{12}C+^{194,198}Pt$. R_C is the parameter for Coulomb radius. V_0, R_0, and a_0 are depth, range, and diffuseness of the real part and V_I, R_I, and a_I are depth, range, and diffuseness of the imaginary part of the optical-model potential used in the code FRESCO [36].

System	V_0 (MeV)	R_0 (fm)	a_0 (fm)	V_I (MeV)	R_I (fm)	a_I (fm)	R_C (fm)
$^{12}C+^{194}Pt$	51.0	1.184	0.630	5.0	0.9	0.2	1.3
$^{12}C+^{198}Pt$	45.0	1.184	0.630	5.0	0.9	0.2	1.3

and Winther (Table VI) [37]. The depth V_0 of the real part of the optical potential was varied to obtain a good fit to the elastic scattering (plus inelastic to low-lying target states) angular distribution. A Woods-Saxon squared imaginary potential that serves to absorb flux penetrating inside the radius R_B and not on the surface, is also listed in Table VI. The optical potentials for elastic, inelastic, and transfer channels were assumed to be the same. The results of the calculations are compared with the experimental values in Figs. 3, 4, 10, 11, 16, and 17 for $^{12}C+^{194,198}Pt$. The effect of different channels included in the calculation on fusion cross sections is also indicated in Figs. 3 and 4 for $^{12}C+^{194}Pt$ and $^{12}C+^{198}Pt$, respectively. It is clear from the two figures that removal of transfer channels has negligible effect on the fusion cross sections. Hence the influence of transfer channels is negligible in the present case.

IV. CONCLUSION

A complete experimental investigation of the $^{12}C+^{194,198}Pt$ systems has been made over the energy range $0.9 \leqslant E/V_B \leqslant 1.2$ MeV. The first moment of CN angular momentum distributions has been deduced from the ratio of ERs. The fusion cross sections for $^{12}C+^{198}Pt$ are found to be smaller than those for $^{12}C+^{194}Pt$ at energies close to the barrier. Simplified coupled-channels calculations have been performed to explain the measured fusion data. The strengths of transfer form factors for $^{12}C+^{194,198}Pt$ have been deduced from the measured transfer angular distributions. The simplified coupled channels calculation including all important inelastic and nucleon-transfer channels adequately explains the observed enhancement in the fusion cross sections and the broadening of the angular-momentum distribution as compared to the one-dimensional barrier-penetration model. The strength of transfer form factors that contain the spectroscopic information is similar for both the systems and is weakly coupled to the entrance channel. The difference in sub-barrier fusion cross sections between $^{12}C+^{194,198}Pt$ systems is due to different collective degrees of freedom associated with the target nuclei. The coupled-reaction-channel calculations including important inelastic channels (2^+, 3^- states of the target and projectile) and transfer channels (one-neutron pickup and one-proton stripping) have been performed. These calculations explain simultaneously the fusion, transfer, and elastic data (plus inelastic to low-lying target states) and also show the role of transfer channels to be negligible in affecting the sub-barrier fusion enhancement. The experimental fusion-barrier distributions deduced from the fusion data are in good agreement with the coupled-channels calculations for both the systems. Comparison of calculations including higher-order coupling terms indicates that projectile excitation does not give rise to a prominent higher-energy peak in the barrier distribution. The distribution of fusion barriers obtained from the quasielastic data for $^{12}C+^{198}Pt$ is broader than those deduced from the fusion data and the coupled-channels calculations.

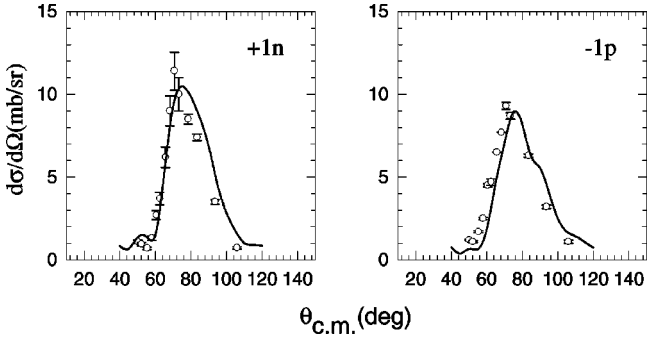

FIG. 16. Transfer angular distribution for one-neutron pickup and one-proton strip-off reactions measured at $E_{lab}=73.5$ MeV for $^{12}C+^{194}Pt$. Solid curve is the result of CRC calculation using the code FRESCO [36].

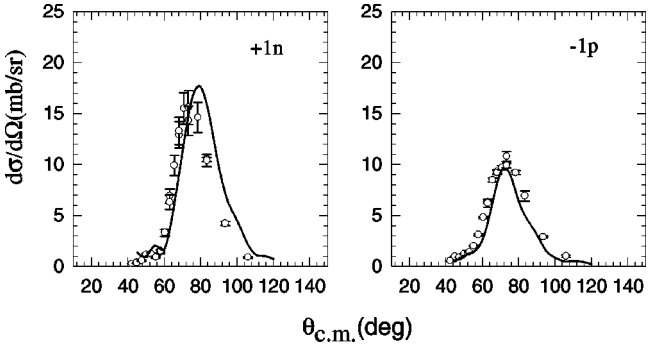

FIG. 17. Same as Fig. 16, for $^{12}C+^{198}Pt$.

In the present case where only one- and two-nucleon transfer reactions are important, the results clearly indicate that coupling to the collective degrees of freedom is the most dominant mechanism in influencing the fusion cross sections at energies near the fusion barrier for $^{12}C+^{194,198}Pt$ systems. This is the first example involving two isotopes of a given target where it is clearly demonstrated that the lighter isotope that is more collective in terms of deformation is the one that exhibits more enhancement of fusion cross section at near-barrier energies as compared to the heavier isotope.

ACKNOWLEDGMENTS

The authors thank the Pelletron accelerator staff for smooth running of the machine. They are grateful to Professor R. Vandenbosch, Professor C.V.K. Baba, and Dr. M. Dasgupta for useful discussions. They are thankful to Dr. B.K. Nayak for helping in the semiclassical transfer reaction analysis. They also thank Dr. S.B. Manohar for his involvement in the early stages of this work.

[1] A. B. Balantekin and N. Takigawa, Rev. Mod. Phys. **70**, 77 (1998).
[2] R. G. Stokstad, Y. Eisen, S. Kaplanis, D. Pelte, U. Smilansky, and I. Tserruya, Phys. Rev. Lett. **41**, 465 (1978); Phys. Rev. C **21**, 2427 (1980); **23**, 281 (1981).
[3] W. Reisdoef, J. Phys. G **20**, 1297 (1994).
[4] M. Beckerman, Rep. Prog. Phys. **52**, 1047 (1988).
[5] A. A. Sonzogni, J. D. Bierman, M. P. Kelly, J. P. Lestone, J. F. Liang, and R. Vandenbosch, Phys. Rev. C **57**, 722 (1998).
[6] H. Timmers, D. Ackermann, S. Beghini, L. Corradi, J. H. He, G. Montagnoli, F. Scarlassara, A. M. Stefanini, and N. Rowley, Nucl. Phys. **A633**, 421 (1998).
[7] A. M. Stefanini, D. Ackermann, L. Corradi, J. H. He, G. Montagnoli, S. Beghini, F. Scarlassara, and G. F. Segato, Phys. Rev. C **52**, R1727 (1995).
[8] A. M. Stefanini, J. Phys. G **23**, 1401 (1997).
[9] A. M. Stefanini, L. Corradi, A. M. Vinodkumar, Yang Feng, F. Scarlassara, G. Montagnoli, S. Beghini, and M. Bisogno, Phys. Rev. C **62**, 014601 (2000).
[10] A. Bohr and B. R. Mottelson, *Nuclear Structure* (Benjamin, Reading, MA, 1975), Vol. II.
[11] R. H. Spear, At. Data Nucl. Data Tables **42**, 55 (1989); S. Raman, C. H. Malarkey, W. T. Milner, C. W. Nestor, Jr., and P. H. Stelson, *ibid.* **36**, 1 (1987).
[12] C. V. K. Baba, V. M. Datar, K. E. G. Löbner, A. Navin, and F. J. Schindler, Phys. Lett. B **338**, 147 (1994).
[13] D. R. Napoli, A. M. Stefanini, H. Moreno Gonzalez, B. Million, G. Prete, P. Spolaore, M. Narayanswamy, Zi Chang Li, S. Beghini, G. Montagnoli, F. Scarlassara, G. F. Segato, C. Signorini, F. Soramel, G. Pollarolo, and C. Rapisarda, Nucl. Phys. **A559**, 443 (1993).
[14] J. Fernandez Niello, C. H. Dasso, and S. Landowne, Comput. Phys. Commun. **54**, 409 (1989).
[15] M. Dasgupta, D. J. Hinde, N. Rowley, and A. M. Stefanini, Annu. Rev. Nucl. Part. Sci. **48**, 401 (1998).
[16] N. Rowley, G. R. Satchler, and P. H. Stelson, Phys. Lett. B **254**, 25 (1991).
[17] H. Timmers, J. R. Leigh, M. Dasgupta, D. J. Hinde, R. C. Lemmon, J. C. Mein, C. R. Morton, J. O. Newton, and N. Rowley, Nucl. Phys. **A584**, 190 (1995).
[18] N. Rowley, H. Timmers, J. R. Leigh, M. Dasgupta, D. J. Hinde, J. C. Mein, C. R. Morton, and J. O. Newton, Phys. Lett. B **373**, 23 (1996).
[19] K. Hagino, N. Takigawa, M. Dasgupta, D. J. Hinde, and J. R. Leigh, Phys. Rev. Lett. **79**, 2014 (1997).
[20] A. Shrivastava, S. Kailas, A. Chatterjee, A. M. Samant, A. Navin, P. Singh, S. Santra, K. Mahata, B. S. Tomar, and G. Pollarolo, *Proceedings of the 9th International Conference on Nuclear Reaction Mechanisms*, Varenna, 2000, edited by E. Gadioli (Ricerca Scientifica ed Educazione Permanente, Milano, 2000), p. 381.
[21] G. Pollarolo and A. Winther, Phys. Rev. C **62**, 054611 (2000).
[22] A. Shrivastava, S. Kailas, A. Chatterjee, A. M. Samant, A. Navin, P. Singh, and B. S. Tomar, Phys. Rev. Lett. **82**, 699 (1999).
[23] K. Shima, T. Ishara, T. Miyoshi, T. Momoi, and T. Mukomo, Phys. Rev. A **29**, 1763 (1984).
[24] J. van der Plicht, H. C. Britt, M. M. Fowler, Z. Frankel, A. Gavron, J. B. Wilhelmy, F. Plasil, T. C. Awes, and G. R. Young, Phys. Rev. C **28**, 2022 (1983).
[25] A. Gavron, Phys. Rev. C **21**, 230 (1980).
[26] M. Dasgupta, A. Navin, Y. K. Agarwal, C. V. K. Baba, H. C. Jain, M. L. Jhingan, and A. Roy, Phys. Rev. Lett. **66**, 1414 (1991).
[27] L. C. Northcliff and R. F. Schilling, Nucl. Data, Sect. A **7**, 233 (1970).
[28] L. Jarczyk, B. Kamys, Z. Rudy, A. Strazalkowski, H. Witała, M. Hugi, J. Lang, R. Müller, J. Sromicki, and H. H. Wolter, Phys. Rev. C **28**, 700 (1983); G. Van der Steenhoven, H. P. Blok, E. Jans, M. De Jong, L. Lapikas, E. N. M. Quint, and P. K. A. De Witt Huberts, Nucl. Phys. **A480**, 547 (1988); Agda Artna-Cohen, Nucl. Data Sheets **83**, 921 (1998); Zhou Chunmei, *ibid.* **57**, 1 (1989); M. R. Schmorak, *ibid.* **53**, 331 (1988).
[29] C. H. Dasso, S. Landowne, and A. Winther, Nucl. Phys. **A405**, 381 (1983); **A407**, 221 (1983).
[30] C. H. Dasso and S. Landowne, Comput. Phys. Commun. **46**, 187 (1987).
[31] R. A. Broglia and A. Winther, *Heavy Ion Reactions* (Addison-Wesley, Redwood City, CA, 1991), Vol. 1.
[32] P. Schwandt, Indiana University Cyclotron Facility Report, SNOOPY, 1984 (unpublished).
[33] L. Corradi, S. J. Skora, U. Lenz, K. E. G. Löbner, P. R. Pascholati, U. Quade, K. Rudolph, W. Schomburg, M. Steinmaya, H. G. Thies, G. Montagnoli, D. R. Napoli, A. M. Stefanini, A. Tivelli, S. Beghini, F. Scarlassara, C. Signorini, and F. Soramel, Z. Phys. A **334**, 55 (1990).
[34] S. Saha, Y. K. Aggarwal, and C. V. K. Baba, Phys. Rev. C **49**, 2578 (1994).
[35] A. Navin, A. Chatterjee, S. Kailas, A. Shrivastava, P. Singh, and S. S. Kapoor, Phys. Rev. C **54**, 767 (1996).
[36] I. J. Thomson, Comput. Phys. Rep. **7**, 167 (1988).
[37] R. A. Broglia and A. Winther, *Heavy Ion Reactions, Lecture Notes* (Benjamin, New York, 1981), Vol. 1.